JOC Article

# Mapping the Triplet Potential Energy Surface of 1-Methyl-8-nitronaphthalene

Svetlana V. Kombarova and Yuri V. Il'ichev*

*Department of Chemistry, Wichita State University, 1845 Fairmount, Wichita, Kansas 67260-0051*

*yuri.ilitchev@wichita.edu*

*Received May 9, 2005*

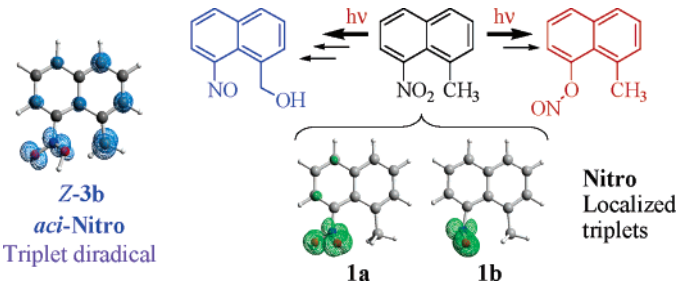


Spin-unrestricted calculations and time-dependent DFT were used to characterize structure and reactivity of 1-methyl-8-nitronaphthalene (**1**) in the triplet state. Four hybrid models (B3LYP, PBE0, MPW1K, BHLYP) with significantly different amount of the exact exchange were employed. The triplet potential energy surface of **1** was mapped by using the UB3LYP and UMPW1K techniques. Both hybrid models provided qualitatively consistent pictures for the potential energy landscape. Thirty-one stationary points, of which 15 were minima, were found at the UB3LYP level of theory. Three minima corresponding to the nitro form of **1** were located on the triplet surface; just one was found for the singlet ground state. Two reaction paths leading from **1** either to a nitrite-type intermediate (**2**) or to the *aci*-form (**3**) were characterized. For both paths, reaction products were of diradical nature. The lower activation energy was obtained for the triplet-state tautomerization affording **3**. The ground state of triplet multiplicity was predicted for two isomers of the *aci*-form. The triplet diradical **3** is expected to react through the thermal population of a close-lying singlet excited state. The results are discussed in relation to mechanisms of photoinduced rearrangements of *peri*-substituted nitronaphthalenes that can be used to develop novel photolabile protecting groups.

## Introduction

Photochemistry of nitro compounds has been attracting considerable attention over many years.[1,2] Among aromatic compounds, 2-nitrobenzyl (2NB) derivatives have enjoyed the widest application. The 2NB functionality is widely used as a photolabile protecting group in organic synthesis,[3−7] polymer chemistry,[8] microelectronics,[9] and biomedical research.[10−17] Photoinduced isomerization of 2NB derivatives is initiated by fast tautomerization that

* To whom correspondence should be addressed. Tel: (316) 978-5702. Fax: (316) 978-3431.

(1) Morrison, H. A. In *The Chemistry of Functional Groups, The Chemistry of the Nitro and Nitroso Groups;* Feuer, H., Ed.; Wiley & Sons: New York, 1969; Chapter 4.

(2) Döpp, D. In: *CRC Handbook of Organic Photochemistry and Photobiology*; Horspool, W. M., Song, P.-S., Eds.; CRC Press: Boca Raton, 1995; pp 1019−1062.

(3) Pillai, V. N. R. *Synthesis* **1980**, 1−26 and references therein.

(4) Barltrop, J. A.; Plant, P. J.; Schofield, P. *J. Chem. Soc., Chem. Commun.* **1966**, 822−823.

(5) (a) Patchornik, A.; Amit, B.; Woodward, R. B. *J. Am. Chem. Soc.* **1970**, *92*, 6333−6335. (b) Zehavi, U.; Amit, B.; Patchornik, A. *J. Org. Chem.* **1972**, *37*, 2281−2285.

(6) (a) Hébert, J.; Gravel, D. *Can. J. Chem.* **1974**, *52*, 187−189. (b) Gravel, D.; Murray, S.; Ladouceur, G. *J. Chem. Soc., Chem. Commun.* **1985**, 1828−1829.

(7) (a) Rich, D. H., Gurwara, S. K. *J. Am. Chem. Soc.* **1975**, *97*, 1575−1579. (b) Rodebaugh, R.; Fraser-Reid, B.; Geysen, H. M. *Tetrahedron Lett.* **1997**, *38*, 7653−7656. (c) Whitehouse, D. L., Savinov, S. N.; Austin, D. J. *Tetrahedron Lett.* **1997**, *38*, 7851−7652.

(8) Beecher, J. E.; Cameron, J. F.; Fréchet, J. M. J. *J. Mater. Chem.* **1992**, *2*, 811−816 and references therein.

(9) (a) Kubota, S.; Tanaka, Y.; Moriwaki, T.; Eto, S. *J. Electrochem. Soc.* **1991**, *138*, 1080−1084. (b) Houlihan, F. M.; Nalamasu, O.; Kometani, J. M.; Reichmanis, E. *J. Imaging Sci. Technol.* **1997**, *41*, 35−40.

(10) Kaplan, J. H.; Forbush, B.; Hoffman, J. F. *Biochemistry* **1978**, *17*, 1929−1935.

(11) For reviews, see: *Methods Enzymol.* **1998**, *291*, 1−259 and references therein.

(12) Pelliccioli, A. P.; Wirz, J. *Photochem. Photobiol. Sci.* **2002**, 1, 441−458 and references therein.

(13) (a) Lester, H. A.; Nerbonne, J. M. *Annu. Rev. Biophys. Bioeng.* **1982**, *11*, 151−175. (b) Gurney, A. M.; Lester, H. A. *Physiol. Rev.* **1987**, *67*, 583−617.

10.1021/jo0509253 CCC: $30.25 
Published on Web 06/22/2005

affords a quinonoid intermediate (also known as nitronic acid or *aci*-form). The subsequent dark reactions that lead to nitroso compounds appeared to be rather complex. Recently, a comprehensive mechanism involving several catalytic steps has been proposed.[18] In addition, a unique competing pathway has been identified for 2NB derivatives with a labile hydrogen in the α-position. Our computational[19] and experimental data[20] provided evidence for the formation of a nitroso hydrate via double hydrogen transfer in 2NB amines and alcohols.

The numerous data available for the 2NB derivatives show that anionic species, which are easily formed from moderately strong nitronic acids in protic solvents, are much less reactive than the protonated form. It is a relatively simple matter to accelerate the *aci*-form decay by using general and specific acid catalysis. Unfortunately, it does not necessarily mean that the protected group release will be accelerated to the same extent. In other words, the release rate is typically much slower than the *aci*-form decay due to a cyclization reaction.[12,18,19] Considering numerous advantages of 2-nitrobenzyl photochemistry,[8,11,12] it would be of great interest to develop an analogous photolabile system that is characterized by a higher rate and quantum efficiency of the protected group release. Several years ago, we proposed to use *peri*-substituted nitronaphthalenes as superior phototriggers.[21] The diradical character of the *aci*-form is of primary importance for defining the photoreactivity of *peri*-substituted nitronaphthalenes. These compounds are expected to undergo a similar reaction as 2NB derivatives, but to form diradical nitronic acids with much more reactive anions. Our preliminary data[21] showed that derivatives of 1-methyl-8-nitronaphthalene with a releasing group in the α-position are characterized by higher quantum yields and higher rates of the product formation than the 2NB analogues. This was confirmed by a recent study of photodecomposition of thymidine 5′-protected carbonates.[22] Although only photolysis times for standardized conditions were reported, the results clearly demonstrated enhanced photoreactivity of *peri*-substituted naphthalenes in comparison to their analogues substituted in the *ortho*-position and 2NB derivatives.

**SCHEME 1. Two Reaction Pathways for Photoisomerization of 1-Methyl-8-nitronaphthalene (1)**

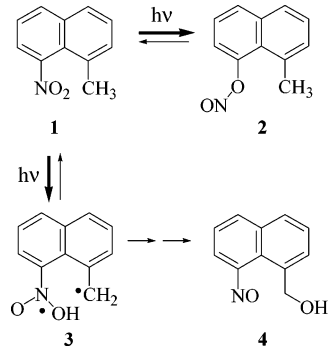


Interest in the photochemistry of nitronaphthalenes was rekindled in the past decade because of related environmental problems. These chemicals are among the most abundant aromatic compounds found in atmosphere.[23] Gas-phase photolysis resulting in the formation of oxygenated compounds, such as quinones, is considered to be the major degradation pathway for these compounds.[24−26] Analogous products were detected upon photodecomposition of 2-substituted-1-nitronaphthalenes in solution.[2,27,28] These results are in clear contrast with early observations indicating that 1-nitronaphthalene (1NN) shows no detectable phototransformation in alcohol solution.[29] It has to be pointed out that 1NN derivatives with a methyl group in the *peri*- or *ortho*-position were found to degrade upon photoirradiation much faster than 1NN and other isomeric methylnitronaphthalenes.

Isomerization of substituted nitronaphthalenes may proceed by several different mechanisms. For photoinduced reactions of compounds bearing a functionalized alkyl group in the *peri*-position, the most likely primary processes are the nitro-nitrite rearrangement and intramolecular hydrogen abstraction. Scheme 1 shows the parent compound, 1-methyl-8-nitronaphthalene (**1**), and its isomers that are formed through these two reactions. Considering that nitro compounds typically show high quantum yields of the triplet formation, it is of great interest to explore the landscape of the triplet-state potential energy surface in relation to photoisomerization mechanisms and potential applications.

## Methods

All calculations were performed with the GAUSSIAN 03 package of programs.[30] Geometries were fully optimized at the B3LYP level of theory with the standard 6-31G(d) basis set. Unrestricted formalism was used for the triplet-state structures and the singlet-state *aci*-form isomers. Selected structures were also optimized by using the 6-31+G(d,p) basis set

(14) (a) McCray, J. A.; Herbette, L.; Kihara, T.; Trentham, D. R. *Proc. Natl. Acad. Sci. U.S.A.* **1980**, *77*, 7237−7241. (b) Walker, J. W.; Reid, G. P.; McCray, J. A.; Trentham, D. R. *J. Am. Chem. Soc.* **1988**, *110*, 7170−7177. (c) Barth, A.; Hauser, K.; Maentele, W.; Corrie, J. E. T.; Trentham, D. R. *J. Am. Chem. Soc.* **1995**, *117*, 10311−10316. (d) Barth, A.; Corrie, J. E. T.; Gradwell, M. J.; Maeda, Y.; Maentele, W.; Meier, T.; Trentham, D. R. *J. Am. Chem. Soc.* **1997**, *119*, 4149−4159.

(15) McCray, J. A.; Trentham, D. R. *Annu. Rev. Biophys. Biophys. Chem.* **1989**, *18*, 239−270.

(16) Adams, S. R.; Tsien, R. Y. *Annu. Rev. Physiol.* **1993**, *55*, 755−784.

(17) Givens, R. S.; Conrad, P. G., II; Yousef, A. L.; Lee, J.-I. In *CRC Handbook of Organic Photochemistry and Photobiology*, 2nd ed.; Horspool, W., Lenci, F., Eds.; CRC Press: Boca Raton, 2004; pp 69/1−69/46.

(18) Il'ichev, Yu. V.; Schwörer, M.; Wirz, J. *J. Am. Chem. Soc.* **2004**, *126*, 4581−4595.

(19) Il'ichev, Yu. V. *J. Phys. Chem. A* **2003**, *107*, 10159−10170.

(20) Gaplovsky, M.; Il'ichev, Yu. V.; Kamdzhilov, Y.; Kombarova, S. V.; Mac, M.; Schwörer, M. A.; Wirz, J. *Photochem. Photobiol. Sci.* **2005**, *4*, 33−42.

(21) Il'ichev, Yu. V.; Simon, J. D.; Wirz J. *Abstracts of Pacifichem 2000*; Honolulu, Hawaii, Dec14−19, 2000; ORGN1049.

(22) Buehler, S.; Lagoja, I.; Giegrich, H.; Stengele, K.-P.; Pfleiderer, W. *Helv. Chim. Acta* **2004**, *87*, 620−659.

(23) Zielinska, B.; Arey, J.; Atkinson, R.; McElroy, P. A. *Environ. Sci. Technol.* **1989**, *23*, 723−729. (b) Arey, J.; Zielinska, B. *J. High Res. Chromatogr.* **1989**, *12*, 101−105.

(24) Feilberg, A.; Kamens, R. M.; Strommen, M. R.; Nielsen, T. *Polycyc. Arom. Comput.* **1999**, *14−15*, 151−160.

(25) Warner, S. D.; Farant, J.-P.; Butler, I. S. *Chemosphere* **2004**, *54*, 1207−1215.

(26) Phousongphouang, P. T.; Arey, J. *J. Photochem. Photobiol., A* **2003**, *157*, 301−309.

(27) Patel, J. R.; Boyer, J. H. *Chemosphere* **1980**, *9*, 99−103.

(28) Döpp, D.; Wong, C. C. *Chem. Ber.* **1988**, *121*, 2045−2047.

(29) (a) Hurley, R.; Testa, A. C. *J. Am. Chem. Soc.* **1968**, *90*, 1949−1952. (b) Trotter, W.; Testa, A. C. *J. Phys. Chem.* **1970**, *74*, 845−847.

in combination with one of the three hybrid functionals: B3LYP, PBE0, and MPW1K. Single-point energies were computed for these geometries by using the same functionals with the 6-311++G(3df,2p) basis set. In addition, the BHLYP/6-311++G(3df,2p) single-point energies were calculated at the B3LYP geometries. B3LYP and BHLYP are combinations of Becke's three-parameter exchange functional[31] (B3) and the half-and-half functional (BH) with the slightly modified Lee−Yang−Parr (LYP)[32] correlation functional. It has to be noted that the BH functional implemented in GAUSSIAN and denoted as BHandH is somewhat different from the original Becke's functional.[33] PBE0 model (also referred to as PBE1PBE) is a combination of the exact exchange (25%) with the Perdew-Burke-Ernzerhof exchange (PBE1) and correlation functionals (PBE).[34,35] MPW1K refers to a method that is based on the modified Perdew-Wang 1991 exchange functional (MPW) and the Perdew−Wang 1991 gradient-corrected correlation functional (PW91).[36] The MPW1K method was specifically optimized for kinetics and contains 42.8% of the Hartree−Fock exchange.[37]

Transition structures (TS) were located by using the GAUSSIAN facility for the synchronous transit-guided quasi-Newton method.[38] Reaction pathways were computed to verify the connection of the TS to the local minima. The intrinsic reaction coordinate (IRC) method[39] was used to trace the steepest-descent paths toward the reactants and the products. A normal vibrational mode corresponding to the single imaginary frequency was inspected to provide additional verification. For all stationary points found in this study, the wave function stability was tested and harmonic vibrational frequencies were calculated using the analytical second derivatives. Cartesian coordinates for the stationary points are available as Supporting Information. Relative energies of different isomers were calculated from their single-point energies corrected to the scaled zero-point vibrational energies (sZPE). For the B3LYP and PBE0 methods, a scaling factor of 0.9806[40] was used for both basis sets employed in this study, ZPE's obtained with the MPW1K technique were scaled with a factor of 0.9515.[41]

## Results

**Molecular Geometry of 1 in the Singlet and Triplet State.** The B3LYP-optimized geometry of 1-methyl-8-nitronaphthalene in the singlet ground state (**1**) is depicted in Figure 1. The atom numbering is also shown in this figure. The same minimum-energy structure was obtained when various initial geometries differing in the configuration of the $NO_2$ and Me groups were used.

There is hardly any difference in the B3LYP bond lengths and angles predicted with 6-31G(d) and 6-31+G(d,p) basis sets (see the Supporting Information). However, adding diffuse functions on the heavy atoms resulted in a larger torsion angle for the C−N bond ($C_9C_8N_{21}O_{22}$: 52.2° and 55.6° for 6-31G(d) and 6-31+G(d,p)). Although all hybrid methods with the 6-31+G(d,p) basis set yielded very similar results for the molecular geometry, the overall better agreement with available X-ray data[42,43] was obtained with the MPW1K model. The B3LYP and PBE0 methods generally overestimated the bond lengths by 1−2% in comparison to the MPW1K technique. However, the N−O bond lengths predicted with these two functionals appeared to be in better agreement with the X-ray data for nitronaphthalenes[42,43] than the MPW1K values.

The naphthalene rings in **1** were predicted to be close to planarity (the dihedral angle deviations within 7°). The $C_{11}$ and N atoms were somewhat displaced from the naphthalene plane and the $C_8$ atom was only slightly off a plane formed by the $NO_2$ group. The exocyclic C−C and C−N bonds were bent outward (away from each other). The C−C bonds in the ring system of **1** (see Figure 1 and the Supporting Information) showed alteration that is typical for naphthalene derivatives. The $C_6$−$C_7$ and $C_7$−$C_8$ bond distances in the range 1.391−1.409 and 1.353−1.362 Å have been reported for crystal structures of *peri*-substituted 8-nitronaphthalenes.[43] The experimental values compare well with corresponding distances of 1.401 Å and 1.365 Å provided by the MPW1K computations. The DFT methods predicted the symmetrical $NO_2$ group rotated by more than 50° out of the naphthalene plane. The torsion angles in the range 45−47° have been reported for 1,8-dinitronaphthalene and 1,4,5,8-tetranitronaphthalene.[43] A dipole moment of 4.3 D predicted for **1** at the B3LYP/6-31+G(d,p) level of theory is close to an experimental value of 4.1 D[44] reported for 1-nitronaphthalene (1NN).

Unrestricted formalism was used for triplet geometry optimization. Three minima ($^3$**1a**−$^3$**1c**) corresponding to the nitro form were located on the triplet potential energy surface by using the UB3LYP and UPBE0 techniques. All minima were characterized by stable wave functions. The geometry optimization using the UMPW1K method in combination with the 6-31+G(d,p) basis set failed to converge for $^3$**1b**. The UMPW1K/6-31G(d) geometry op-

(30) Gaussian 03, Revision C.02. Frisch, M. J.; Trucks, G. W.; Schlegel, H. B.; Scuseria, G. E.; Robb, M. A.; Cheeseman, J. R.; Montgomery, J. A., Jr.; Vreven, T.; Kudin, K. N.; Burant, J. C.; Millam, J. M.; Iyengar, S. S.; Tomasi, J.; Barone, V.; Mennucci, B.; Cossi, M.; Scalmani, G.; Rega, N.; Petersson, G. A.; Nakatsuji, H.; Hada, M.; Ehara, M.; Toyota, K.; Fukuda, R.; Hasegawa, J.; Ishida, M.; Nakajima, T.; Honda, Y.; Kitao, O.; Nakai, H.; Klene, M.; Li, X.; Knox, J. E.; Hratchian, H. P.; Cross, J. B.; Bakken, V.; Adamo, C.; Jaramillo, J.; Gomperts, R.; Stratmann, R. E.; Yazyev, O.; Austin, A. J.; Cammi, R.; Pomelli, C.; Ochterski, J. W.; Ayala, P. Y.; Morokuma, K.; Voth, G. A.; Salvador, P.; Dannenberg, J. J.; Zakrzewski, V. G.; Dapprich, S.; Daniels, A. D.; Strain, M. C.; Farkas, O.; Malick, D. K.; Rabuck, A. D.; Raghavachari, K.; Foresman, J. B.; Ortiz, J. V.; Cui, Q.; Baboul, A. G.; Clifford, S.; Cioslowski, J.; Stefanov, B. B.; Liu, G.; Liashenko, A.; Piskorz, P.; Komaromi, I.; Martin, R. L.; Fox, D. J.; Keith, T.; Al-Laham, M. A.; Peng, C. Y.; Nanayakkara, A.; Challacombe, M.; Gill, P. M. W.; Johnson, B.; Chen, W.; Wong, M. W.; Gonzalez, C.; and Pople, J. A.; Gaussian, Inc., Wallingford CT, 2004.

(31) Becke, A. D. *J. Chem. Phys.* **1993**, *98*, 5648−5652.

(32) (a) Lee, C.; Yang, W.; Parr, R. G. *Phys. Rev. B* **1988**, *37*, 785−797. (b) Stephens, P. J.; Devlin, F. J.; Chabalowski, C. F.; Frisch M. J. *J. Phys. Chem.* **1994**, *98*, 11623−11627.

(33) Becke, A. D. *J. Chem. Phys.* **1993**, *98*, 1372−1377.

(34) (a) Perdew, J. P.; Burke, K.; Ernzerhof, M. *Phys. Rev. Lett.* **1996**, *77*, 3865−3868. (b) Perdew, J. P.; Burke, K.; Ernzerhof, M. *Phys. Rev. Lett.* **1997**, *78*, 1396−1396.

(35) (a) Adamo, C.; Barone, V. *Chem. Phys. Lett.* **1998**, *298*, 113−119. (b) Adamo, C.; Barone, V. *J. Chem. Phys.* **1999**, *110*, 6158−6170. (c) Ernzerhof, M.; Scuseria, G. E. *J. Chem. Phys.* **1999**, *110*, 5029−5036.

(36) (a) Perdew, J. P.; Wang, Y. *Phys. Rev.* **1992**, *B45*, 13244−13255. (b) Perdew, J. P.; Chavary, J. A.; Vosko, S. H.; Jackson, K. A.; Pederson, M. R.; Singh, D. J.; Fiolhais, C. *Phys. Rev.* **1992**, *B46*, 6671−6679.

(37) Lynch, B. J.; Fast, P. L.; Harris, M.; Truhlar, D. G. *J. Phys. Chem. A* **2000**, *104*, 4811−4815.

(38) Peng, C.; Schlegel, H. B. *Isr. J. Chem.* **1993**, *33*, 449−454.

(39) (a) Fukui, K. *Acc. Chem. Res.* **1981**, *14*, 363−368. (b) Gonzalez, C.; Schlegel, H. B. *J. Phys. Chem.* **1990**, *94*, 5523−5527.

(40) Scott, A. P.; Radom, L. J. *J. Phys. Chem.* **1996**, *100*, 16502−16513.

(41) Lynch, B. J.; Truhlar, D. G. *J. Phys. Chem. A.* **2001**, *105*, 2936−2941.

(42) Trotter, J. *Acta Crystallogr.* **1960**, *13*, 95-. (b) Ammon, H. L. *Acta Crystallogr. C* **1991**, *C47*, 2252−2254.

(43) (a) Akopyan, Z. A.; Kitaygorodsky, A. I.; Struchkov, Yu. T. *Zh. Strukt. Khim.* **1965**, *6*, 729-. (b) Holden, J.; Dickinson, C. *Chem. Commun.* **1969**, 144. (c) Ciechanowicz-Rutkowska, M. *J. Solid State Chem.* **1977**, *22*, 185−192. (d) Procter, G.; Britton, D.; Dunitz, J. D. *Helv. Chim. Acta* **1981**, *64*, 471−477.

(44) Bethea, C. G. *J. Chem. Phys.* **1978**, *69*, 1312−1313.

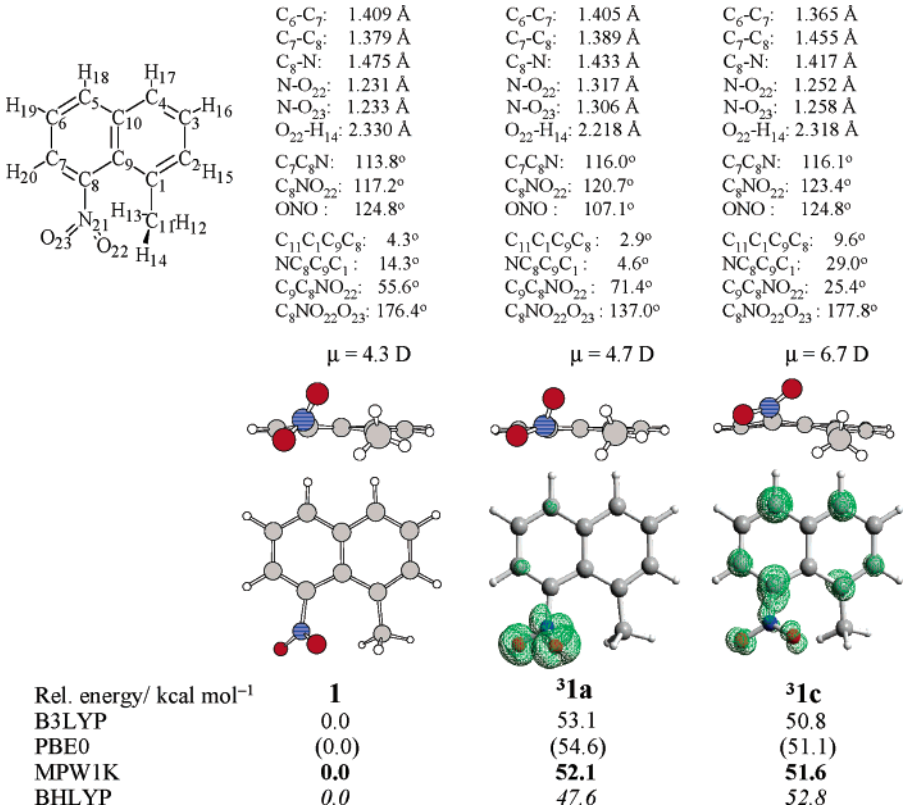


| Rel. energy/ kcal mol$^{-1}$ | **1** | **$^3$1a** | **$^3$1c** |
|---|---|---|---|
| B3LYP | 0.0 | 53.1 | 50.8 |
| PBE0 | (0.0) | (54.6) | (51.1) |
| MPW1K | **0.0** | **52.1** | **51.6** |
| BHLYP | *0.0* | *47.6* | *52.8* |

**FIGURE 1.** B3LYP/6-31+G(d,p)-optimized geometries of 1-methyl-8-nitronaphthalene in the singlet ground state (**1**) and the triplet excited state (**$^3$1a**, **$^3$1b**). Spin-unrestricted calculations were used for triplet species. The atom numbering, selected structural parameters, and dipole moments ($\mu$) are shown. Energies in kcal mol$^{-1}$ relative to that of **1** are also given. These energies were calculated from the single-point energies computed with four different DFT techniques in combination with the 6-311++G-(3df,2p) basis set and were corrected to the scaled zero-point vibrational energies (sZPE) obtained at the same level of theory as the energy, but with the 6-31+G(d,p) basis set. The white circles represent H atoms; the gray circles, C atoms; the red circles, O atoms; and the circles with blue horizontal lines, N atoms. Green wire mesh at the triplet species shows the SCF electron spin density.

timization yielded a structure similar to that obtained at the UB3LYP/6-31G(d) level and denoted as **$^3$1b**, but wave function instability was detected. Figure 1 shows the UB3LYP/6-31+G(d,p) optimized geometries, relative energies, and SCF electron spin densities for **$^3$1a** and **$^3$1c**. The expectation values of the spin angular momentum squared ($S^2$) for these two species were 2.0169 and 2.0207; i.e., their wave functions were not contaminated by higher spin states.

The naphthalene moiety in **$^3$1a** was found to be practically identical to that in **1**. In contrast, the C−N bond length in **$^3$1a** was predicted to be reduced by 2−3% (depending on the method used) relative to that in **1**. The $NO_2$ group with the N−O bonds stretched by 6−8% was strongly bent (see Figure 1). At the UB3LYP level, the $H_{14}$−$O_{22}$ nonbonded distance in **$^3$1a** was found to decrease by ∼5% relative to that in **1**. An $H_{14}$−$O_{22}$ distance of 2.172 Å was predicted for **$^3$1a** with the UMPW1K/6-31+G(d,p) method. This value is by ca. 6% shorter than that in the ground-state species. **$^3$1b** differs from **$^3$1a** only in that the $O_{23}$ atom is displaced from the naphthalene ring plane and both N−O bonds are directed toward the $CH_3$ group. All differences in the bond lengths were within 1%.

The molecular geometry of **$^3$1c** strongly deviates from that of **1** and **$^3$1a**. All DFT methods in combination with the 6-31+G(d,p) basis set predicted a substantial displacement of the atoms located outside the naphthalene ring and a distortion of the ring system (Figure 1). At the B3LYP level, the $C_1$−$C_9$, $C_2$−$C_3$, $C_6$−$C_7$, and $C_8$−N bond lengths in **$^3$1c** were reduced by 2−4% relative to those in **1**. In contrast, the $C_1$−$C_2$, $C_3$−$C_4$, $C_5$−$C_6$, and $C_7$−$C_8$ bonds were elongated by 3−6%. The N−O bonds in **$^3$1c** were found to be only slightly stretched (<2%) in comparison to those in **1**. Similar results for the molecular geometry of **$^3$1c** were obtained with two UPBE0 and UMPW1K techniques. The SCF spin density was found to be almost equally distributed between the $C_1$, $C_4$, $C_5$, and $C_8$ atoms of **$^3$1c**. Significant density was predicted also for $C_2$, $C_7$, and both O atoms. Contrary, only a small fraction of the unpaired spin was localized at the N atom. A large dipole moment of 6.7 D implies that charge-transfer configuration(s) make a significant contribution to the triplet species **$^3$1c**.

At the UB3LYP level, **$^3$1c** with relative energy of 50.8 kcal mol$^{-1}$ was found to be the most stable triplet species. **$^3$1a** and **$^3$1b** were destabilized by 2.3 and 5.6 kcal mol$^{-1}$, respectively. The UPBE0 results for the relative energies were similar to those of the UB3LYP technique. The UMPW1K method yielded practically identical energies for **$^3$1a** and **$^3$1c** (see Figures 1 and 4). When the UBHLYP single-point energies computed at the UB3LYP geometries were used, the energy of **$^3$1c** amounted to 52.8 kcal mol$^{-1}$ and this triplet was by 5.2 kcal mol$^{-1}$ less stable

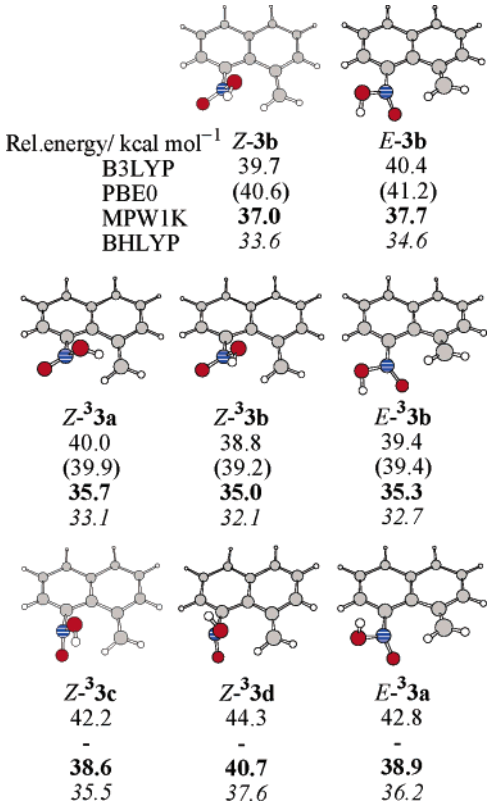


**FIGURE 2.** B3LYP/6-31+G(d,p)-optimized geometries of the *aci*-form stereoisomers (**3**) in the singlet and triplet state. Explanations for the symbols and energy calculations are given in Figure 1. For the three isomers that lack the PBE0 data, the B3LYP/6-31G(d) geometries are presented and single-point energies calculated at these geometries are used in energy calculations.

than $^3$**1a**. It has to be pointed out that the $^3$**1a** dipole moment predicted by the BHLYP technique (3.3 D) was substantially smaller than those obtained with other methods.

***Aci*-Form of 8-Nitro-1-Methylnaphthalene.** An [1,7]H-shift in **1** affords an intermediate (**3**) that is formally analogous to the *aci*-form of 2-nitrobenzyl derivatives. However, no quinonoid structural formula can be assigned to **3** and this species has to be described as a diradical (see Scheme 1). Initial computations for the triplet *aci*-form ($^3$**3**) were performed at the UB3LYP/6-31G(d) level of theory. We located six minima corresponding to stereoisomers and conformers of $^3$**3** with different configurations of the nitronic moiety. The molecular geometries obtained are depicted in Figure 2. Here, *E*- and *Z*- indicate the position of the OH group relative to the methylene group. Geometries of the three isomers with the lowest energy were also optimized using the 6-31+G(d,p) basis set and two other functionals, UPBE0 and UMPW1K. The energies calculated relative to that of **1** are presented in Figure 2.

The diradical intermediates $^3$**3** were predicted to have asymmetric N−O bonds (N−$O_{23}$: 1.257 Å, N−$O_{22}$: 1.433 Å for *Z*-$^3$**3b**, here and below the UB3LYP/6-31+G(d,p) geometries are presented unless otherwise stated). The N−O bond lengths were in the range of the experimental values reported for benzoyl and silyl nitronates (1.232−1.271 and 1.400−1.453 Å).[45]

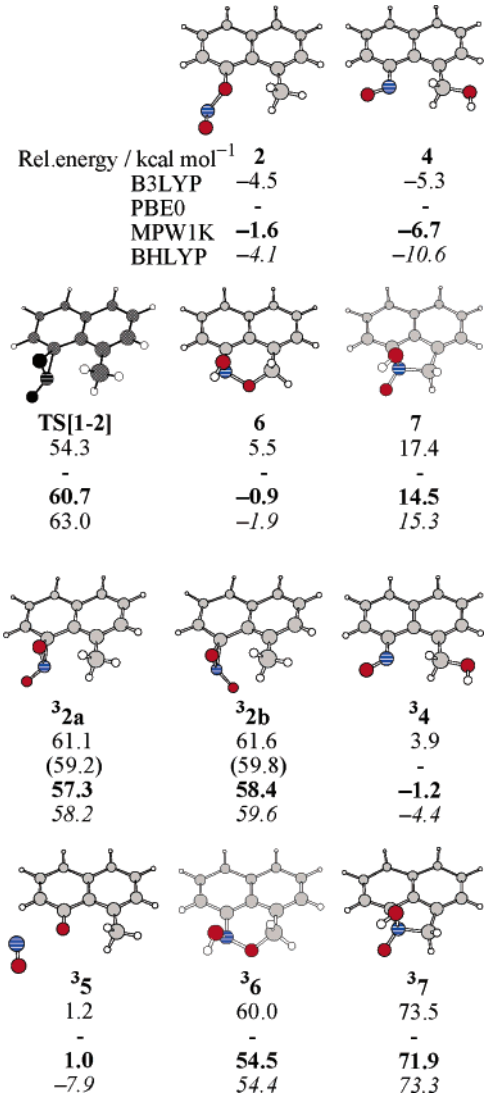


**FIGURE 3.** B3LYP/6-31G(d)-optimized geometries of isomers of 8-nitro-1-methylnaphthalene (**2**−**7**) in the singlet and triplet state. The transition structure for nitro-nitrite rearrangement in the ground state, **TS[1**−**2]**, is also presented. The relative energies (kcal mol$^{-1}$) were calculated from the single-point energies computed with four different DFT techniques in combination with the 6-311++G(3df,2p) basis set and were corrected to sZPE estimated at the B3LYP/6-31G(d) level. For $^3$**2a** and $^3$**2b**, the energies were obtained as described in Figure 1.

It is noteworthy that the C−N bond remained practically unaltered upon [1,7]H-shift in the triplet state. The overall configuration of the nitronic moiety in $^3$**3** resembled that of the bent nitro group in $^3$**1a**. In *Z*-$^3$**3a** and *Z*-$^3$**3b**, the $C_9C_8NO_{22}$ dihedral angle was close to 60° (the $O_{22}$ atom linked to $H_{14}$ is shown above the ring plane in Figure 2). The configuration of *Z*-$^3$**3c** and *Z*-$^3$**3d** with both $C_8NO$ planes being almost perpendicular to the $C_7C_8C_9$ plane was reminiscent of that in $^3$**1b**. Aside from the NOOH group, *E*- and *Z*-$^3$**3b** showed quite similar geometries with the largest discrepancy being reduction of the C−N bond length by 1.5% in the *E*-isomer. Although the electron spin density in *Z*-$^3$**3b** was mainly localized on the NO moiety and the exocyclic $C_{11}$ atom, a large fraction of unpaired spin was found on the $C_2$ and $C_4$ atoms of

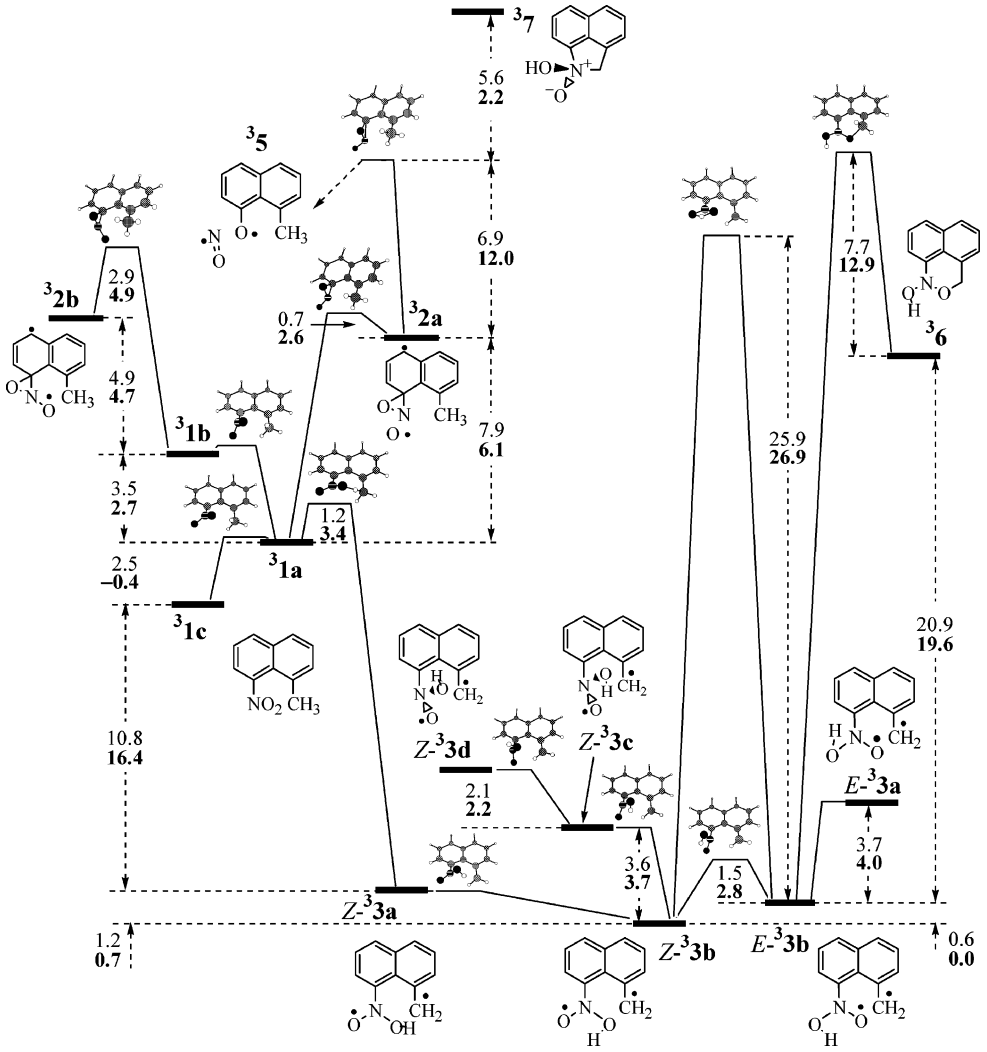


**FIGURE 4.** Schematic profile of the triplet potential energy surface for the isomerization of **1** calculated at the UB3LYP/6-311++G(3df,2p)(+sZPE)//UB3LYP/6-31G(d) level of theory. Values given in bold were obtained from the UMPW1K/6-311++G-(3df,2p) single-point energies computed at the same geometries. All energies are given in kcal mol$^{-1}$.

the naphthalene ring (data not shown). The strong coupling between the methylene group and the naphthalene moiety in all isomers of $^3$**3** was evident from a shortened C−C bond outside of the aromatic ring ($C_1$−$C_{11}$: 1.394 Å and 1.507 Å for *Z*-$^3$**3b** and $^3$**1a**) and essentially planar structure of the $C_1C_{11}H_{12}H_{13}$ moiety.

We located a transition structure for the rotation of the $CH_2$ group in *E*-$^3$**3b** (**TS1[***E*-$^3$**3b**-*E*-$^3$**3b**] in Table 1S, Supporting Information). At the UMPW1K level, the activation energy of 13.4 kcal mol$^{-1}$ was predicted for this rotation. The C−C bond alteration was less pronounced in the ring system of the *aci*-form than of the nitro compound. The naphthalene moiety in the isomers of $^3$**3** only slightly deviates from planarity, the deformation is mainly realized through displacement of the $C_1$ and $C_8$ atoms into the opposite directions. Clearly, the pyramidal configuration of the nitrogen in the NOOH group allows avoiding the close proximity of the O(H) and $CH_2$ groups and minimizing the ring distortion.

All isomers of $^3$**3** were substantially destabilized in comparison to the ground state of the nitro form **1** (Figure 2). The UB3LYP energy of the most favorable isomer, *Z*-$^3$**3b**, amounts to 38.8 kcal mol$^{-1}$. However, this value is significantly smaller than the energy of the triplet nitro compound $^3$**1c**. Interestingly, the *E*-$^3$**3b** was slightly destabilized in comparison to the *Z*-isomer. For 2NB derivatives, the *E*-isomers were typically found to be more stable.[19,46] The cyclic form of *E*-$^3$**3b** with a three-membered ring resembling that in $^3$**2a** (see below) was destabilized by additional 28.1 kcal mol$^{-1}$ as predicted at UB3LYP/6-31G(d) level. Isomers of **3** that did not form an intramolecular H-bond between the OH group and the second O atom were disfavored by 1−3 kcal mol$^{-1}$. Degenerate rearrangement of *E*-$^3$**3b** through flipping of the exocyclic groups was found to encounter a barrier of 5.5 kcal mol$^{-1}$ as predicted at the UB3LYP level (for the TS geometry see **TS2[***E*-$^3$**3b**-*E*-$^3$**3b]** in Table 1S, Supporting Information).

We also attempted to predict geometry and energy of the *aci*-form in the singlet state. The RB3LYP computa-

(45) (a) Powell, D. R.; Hanson, P. E.; Gellman, S. H. *Acta Crystallogr.* **1996**, *C52*, 2945−2946. (b) Colvin, E. W.; Beck, A. K.; Bastani, B.; Seebach, D.; Kai, Y.; Dunitz, J. D. *Helv. Chim. Acta* **1980**, *63*, 697−710.

(46) Il'ichev, Yu. V.; Wirz, J. *J. Phys. Chem. A* **2000**, *104*, 7856−7870.

tions (both closed- and open-shell) for the singlet-state isomers **3** yielded either geometries with unstable wave functions or structures identical to other isomers. Two minimum-energy structures with stable wave functions, *Z*-**3b** and *E*-**3b** (Figure 2), could be located by using unrestricted methods. However, these species were approximately 50% triplets as can be judged from the $S^2$ values of 1.0390 and 1.0134 for the UB3LYP/6-31+G(d,p) wave functions of *Z*-**3b** and *E*-**3b**. The unrestricted wave functions obtained with the UPBE0 and UMPW1K methods were even stronger contaminated by higher spin states. For all isomers of the triplet diradical $^3$**3**, the $S^2$ values for the UB3LYP wave functions were in the range 2.0478−2.0749. Therefore, the triplet wave functions were practically free of contamination. The $S^2$ values obtained at the UPBE0 and UMPW1K level were slightly higher, but still did not exceed the theoretical value by more than 11%.

The UB3LYP geometries of *Z*- and *E*-**3b** were found to only slightly vary when the state multiplicity changed. However, the high spin contamination of the unrestricted singlet wave functions casts some doubts upon the accuracy of the DFT results for the singlet diradicals **3**. The accurate determination of the singlet−triplet energy gap ($\Delta E_{ST} = E_S - E_T$) also appears to be difficult. Relative energies shown in Figure 2 give $\Delta E_{ST}$ values of approximately +1 kcal mol$^{-1}$. Correction for the effects of the spin contamination should only increase these values. If we use a formula proposed by Yamaguchi et al.[47] to correct the UB3LYP singlet-state energies, we obtain $\Delta E_{ST}$ = 1.9 and 2.3 kcal mol$^{-1}$ for *Z*- and *E*-**3b**, respectively.

**Various Isomers of 8-Nitro-1-methylnaphthalene.** This study was focused on the two isomerization pathways leading either to the nitrite **2** or to the nitroso alcohol **4**. The B3LYP/6-31G(d)-optimized geometries for the selected conformers of these two compounds are depicted in Figure 3. For both compounds, the naphthalene moiety with alternating C−C bonds was predicted to be planar. The two exocyclic atoms connected to the rings were located in the same plane. The formally double N=O bond (1.170 Å) and the formally single $C_8-O_{22}$ bond (1.385 Å) in **2** were noticeably shorter than the comparable bonds in **4** ($N-O_{23}$: 1.227 Å, $C_{11}-O_{22}$: 1.425 Å). Sizable lengthening of the second N−O bond in **2** ($N-O_{22}$: 1.485 Å) was also found. The angles formed by the two bonds centered at the N atom differed substantially in **2** and **4** (ONO, 109.8°; CNO, 115.8°).

Three DFT techniques used in this study predicted for the isomers **2** and **4** to be energetically more favorable than the parent compound **1**. The formation of **2** was found to be exothermic by 4.5 and 1.6 kcal mol$^{-1}$ at the B3LYP and MPW1K/6-311++G(3df,2p) level, respectively. At the same level of theory, exothermicity of 5.3 and 6.7 kcal mol$^{-1}$ was found for the reaction **1** → **4**. For the nitro-nitrite rearrangement in the ground state, we located a transition structure, **TS[1−2]**, whose geometry is depicted in Figure 3. This TS is characterized by weak bonding of the $NO_2$ group ($C_8-N$, 1.645 Å; $C_8-O_{22}$, 1.762 Å) and by a relative small elongation of the N−O bond ($N-O_{22}$, 1.325 Å) involved in the rearrangement. A huge activation barrier of 60.7 kcal mol$^{-1}$ was predicted for the reaction **1** → **2** at the MPW1K level. In exploring reaction pathways for the formation of **4**, we obtained optimized geometries for two tricyclic compounds, **6** and **7** (Figure 3), that may arise as intermediates after the [1,7]H-shift in **1**. The *N*-hydroxynaphthoxazine **6** was predicted to be a rather stable compound with the energy comparable to that of **1**. The benzindole derivative **7** was destabilized by 12−15 kcal mol$^{-1}$ relative to **6**.

To elucidate the role of photoexcitation in the two isomerization reaction described above, we optimized geometries and estimated energies of the isomers of **1** in the triplet state. The overall geometry of **4** did not show dramatic changes upon excitation, but substantial changes occurred around the NO group. At the UB3LYP/6-31G(d) level, the C−N bond length is expected to decrease from 1.434 Å in **4** to 1.367 Å in $^3$**4**. The CNO bond angle increases from 115.8° in the ground state to 128.8° in the $T_1$ state of **4**. The localized changes are consistent with the n-$\pi^*$ character of the lowest triplet excited state of the nitroso compound. Both tricyclic intermediates, **6** and **7**, showed considerable geometrical changes in the triplet state. The C−C bonds in the naphthalene ring became more uniform, mainly due to stretching of the shorter bonds ($C_1-C_2$, $C_7-C_8$, etc). The configuration of the NOOH moiety was also altered. At the B3LYP level, the CNO plane is almost perpendicular to the naphthalene plane in the singlet **6** and forms an angle of 69° in $^3$**6**. The N−O(H) bond that was notably elongated in **7** ($N-O_{23}$, 1.568 Å) became practically broken in $^3$**7** ($N-O_{23}$, 1.611 Å). In contrast, the $C_8-N$ bond in the triplet species shrunk by 2.1% in comparison to that in **7**. The energies of $^3$**6** and $^3$**7** relative to the corresponding ground-state species amounted to 54.5 and 56.1 kcal mol$^{-1}$ as predicted at the UB3LYP level.

The UB3LYP geometry optimization that was started at the geometry of **2**, but performed for the triplet state yielded a radical pair $^3$**5** comprised of the NO and 1-methylnaphthoxy radicals. The geometry of $^3$**5** was characterized by $N-O_{22}$ and $N-O_{23}$ distances of 2.736 and 1.160 Å, respectively. The triplet radical pair $^3$**5** was predicted to be exceptionally stable and have energy comparable with that of **1** in the ground state (see Figure 3). Beginning with the TS geometry for the nitro-nitrite rearrangement in the ground-state we were able to locate an analogous transition structure for the triplet-state reaction (see Figure 4 and the Supporting Information for **TS[**$^3$**1a**−$^3$**2a]**). Thereafter we performed an IRC calculation to establish the connectivity of this TS. We found that it was linked to $^3$**1a** and a diradical intermediate $^3$**2a** that was quite different from the nitrite **2**. The geometry of $^3$**2a** optimized at the UB3LYP/6-31+G(d) level is shown in Figure 3. The electron spin density in this diradical was mainly localized on the $C_5$, $C_7$, and exocyclic $O_{23}$ atoms. When the geometry of $^3$**2a** was reoptimized for the singlet state, we obtained a molecule identical to **2**. The oxaziridine ring in $^3$**2a** was perpendicular to the plane of the naphthalene moiety. The UB3LYP/6-31+G(d,p) method yielded lengths of 1.459 and 1.484 Å for the $C_8-N$ and $C_8-O_{22}$ bonds, respectively. The endocyclic $N-O_{22}$ bond in $^3$**2a** was stretched by 14.0%, while the exocyclic $N-O_{23}$ bond contracted by 5.3% relative to the corresponding distances in the reactant, $^3$**1a**. The $C_8NO_{23}$ and $C_8NO_{22}$ bond angles were

(47) Yamaguchi, K.; Jensen, F.; Dorigo, A.; Houk, K. N. *Chem. Phys. Lett.* **1988**, *149*, 537−542.

128.5° and 61.3°, respectively. The $C_7-C_8$ and $C_8-C_9$ bonds were elongated by 4.4% and 6.4% in comparison to those in **$^3$1a**. Generally, the naphthalene ring of **$^3$2a** resembled that of the nitro triplet **$^3$1c** that was compacted along the short pseudoaxis. At the UB3LYP/6-311++G(3df,2p) level, the diradical **$^3$2a** corresponding to the triplet-state "nitrite" is destabilized by 61.1 kcal mol$^{-1}$ relative to **1**. Slightly smaller values were obtained with other three functionals. A stereoisomer with the inverted nitrogen (**$^3$2b**) was destabilized by 0.5−1.4 kcal mol$^{-1}$ relative to **$^3$2a**.

**Potential Energy Profile for Isomerization Reactions.** A potential energy profile for the triplet-state isomerization of 1-methyl-8-nitronaphthalene (Figure 4) was constructed by using the UB3LYP and UMPW1K/6-311++G(3df,2p) single-point energies that were computed at the UB3LYP/6-31G(d) geometries and corrected to the sZPE's. Total energies for all stationary points found are presented in Table 1S of the Supporting Information. IRC calculations performed for all transition structures except those connecting the nitro triplets **$^3$1a**−**$^3$1c** confirmed the connectivity shown in Figure 4. The activation energies that are not labeled in this figure could not be estimated with reasonable accuracy. Generally, the DFT techniques used failed to predict the activation barriers for the OH group rotation in the *aci*-form isomers.

Negative activation energies were obtained for the downhill reactions after correction for sZPE. A similar problem was found for the reaction *Z*-**$^3$3c** → *Z*-**$^3$3b** that proceeds through the nitrogen inversion. "Negative" barriers were also obtained when the UMPW1K optimized geometries were used. However, activation barriers for all these transformations are expected to be rather small and therefore major conclusions made in this study should not be affected by the lack of accurate estimates of the activation barriers.

The UB3LYP/6-31+G(d)-optimized geometries of the TS for the triplet-state tautomerization, **TS[$^3$1a**−*Z*-**$^3$3a]**, and for the nitro-nitrite rearrangements, **TS[$^3$1a**−**$^3$2a]**, are depicted in Figure 5. The reaction and activation energies that were obtained with four different DFT methods for these two competing reactions are also presented in this figure. For all techniques except BHLYP, the single-point energies were computed at the geometries fully optimized with the same functional, but with a smaller basis set. The UBHLYP single-point energies were obtained at the UB3LYP/6-31+G(d,p) geometries.

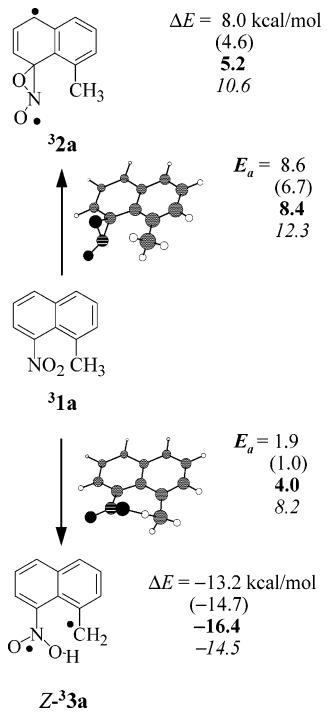


**FIGURE 5.** Triplet-state tautomerization and nitro-nitrite rearrangement of 8-nitro-1-methylnaphthalene studied with different DFT techniques. The 6-31+G(d,p) basis set was used to optimize geometries of the minimum- and transition structures. Energies in kcal mol$^{-1}$ ($\Delta E$, $E_a$) relative to that of **$^3$1a** were calculated using the B3LYP (regular font), PBE0 (values in parentheses), MPW1K (bold), and BHLYP method (italic) in combination with the 6-311++G(3df,2p) basis set. The B3LYP/6-31G(d) geometries were used in the BHLYP computations.

## Discussion

**Triplet Excited States of 1-Methyl-8-nitronaphthalene (1).** The distinctive feature of many aromatic nitro compounds is that triplet states are populated with very high quantum efficiencies and rates. A quantum yield of ~0.6 was reported for the formation of the first triplet excited state of 1NN.[29] The $S_1 \rightarrow T_1$ intersystem crossing in 1NN was characterized by a rate constant of $\sim 10^{11}$ s$^{-1}$.[48] In the absence of the T−T annihilation (low excitation energies), the $T_1$ state of 1NN decayed exponentially with a lifetime that was dependent on solvent. The lifetime ranged from 1 $\mu$s to ~10 $\mu$s at room temperature[49−52] and approached 50 ms at 77 K.[49,53−56] Similar parameters were obtained for the triplet state of 1,8-dinitronaphthalene.[53,57]

The triplet-state lifetime, zero-field splitting parameters, and poor reactivity in hydrogen abstraction reactions indicate that the $T_1$ state of 1NN is mainly $\pi-\pi^*$ in nature. We used the UB3LYP\6-31G(d) method to find geometry of the 1NN triplet. A single geometry with the nitro group positioned in the plane of the naphthalene moiety could be found (see Figure 1S of the Supporting Information).[58] At this level of theory, we obtained a

(48) Anderson, R. W., Jr.; Hochstrasser, R. M.; Lutz, H.; Scott, G. W. *Chem. Phys. Lett.* **1974**, *28*, 153−157.
(49) Kanamaru, N.; Okajima, S.; Kimura, K. *Bull. Chem. Soc. Jpn.* **1972**, *45*, 1273.
(50) Capellos, C.; Porter, G. *J. Chem. Soc., Faraday Trans. 2* **1974**, *70*, 1159−1164.
(51) Tinkler, J. H.; Tavender, S. M.; Parker, A. W.; McGarvey, D. J.; Mulroy, L.; Truscott, T. G. *J. Am. Chem. Soc.* **1996**, *118*, 1756−1761.
(52) Görner, H. *J. Chem. Soc., Perkin Trans. 2* **2002**, 1778−1783.
(53) Khalil, O. S.; Bach, H. G.; McGlynn, S. P. *J. Mol. Spectrosc.* **1970**, *35*, 455−460.
(54) Rusakowicz, R.; Testa, A. C. *Spectrochim. Acta A* **1971**, *27*, 787−792.
(55) Mikula, J. J.; Anderson, R. W.; Harris, L. E.; Stuebing, E. W. *J. Mol. Spectrosc.* 1972, *42*, 350−369.
(56) (a) Shioya, Y.; Yagi, M.; Higuchi, J. *Chem. Phys. Lett.* **1989**, *154*, 25−28. (b) Yagi, M.; Shioya, Y.; Higuchi, J. *J. Photochem. Photobiol. A* **1991**, *62*, 65−73.
(57) Görner, H. *J. Phys. Chem. A* **2002**, *106*, 5989−5998.
(58) Il'ichev, Yu. V. Unpublished results.

dipole moment of 4.7 and 6.7 D for the ground and first triplet excited state, respectively. According to CIS computations,[59] the $T_1$ state is characterized by an increased dipole moment and a reduced twisting angle for the $NO_2$ group as compared to the ground state. The geometry in the second triplet excited state, which is located in close proximity to $T_1$, is characterized by a strongly bent $NO_2$ group.[59] This geometrical perturbation in the $T_2$ state appears to be quite similar to that predicted by CAS−SCF computations for nitrobenzene in the two lowest excited states both of singlet and triplet multiplicity.[60] The N-atom pyramidalization for the nitro group of 2NB derivatives was proposed to be a key factor that determines the extraordinary short lifetime of the $T_1$ state and affects the photoreactivity of these compounds.[61] The $NO_2$ group that is not coplanar with the carbon atom was also predicted for the triplet state of nitromethane.[62] It is noteworthy that similar results for the nitromethane triplet were obtained by using the CAS−SCF and B3LYP method.

Optimized geometries of two triplet species (**$^3$1a**, **$^3$1c**) corresponding to the nitro form of **1** were obtained from unrestricted calculations utilizing three hybrid functionals (B3LYP, PBE0, MPW1K) in combination with either 6-31G(d) or 6-31+G(d,p) basis set. Three methods provided similar geometrical parameters for each molecule and predicted profound structural differences between **$^3$1a** and **$^3$1c**. The geometry of the localized triplet **$^3$1a** resembled that of 1NN in the $T_2$ state and nitrobenzene in the $T_1$ state. We also obtained a similar geometry with the bent $NO_2$ group and largely stretched N−O bonds for the triplet state of 2-nitrotoluene (see Figure 1S, Supporting Information). Pronounced structural changes in the $NO_2$ group are in accord with excitation being mainly localized on this group. The localized radical-like character of **$^3$1a** is demonstrated by the electron spin density almost exclusively distributed over the N and O atoms (Figure 1). The polar triplet **$^3$1c** with the spin density delocalized over the aromatic system matches up with the first triplet excited state of 1NN. The substantial compression along the short pseudoaxis and a reduced torsion angle of the $NO_2$ group in **$^3$1c** are indicative of a stronger coupling between the ring system and the nitro group. These data suggest that **$^3$1a** and **$^3$1c** correspond to the two lowest triplet excited states of **1**. It has to be emphasized that only a single triplet minimum could be located at the UB3LYP/6-31G(d) level both for 1NN and 2-nitrotoluene in the nitro form (Figure 1S, Supporting Information).

To elucidate the nature of triplet species found for the nitro form of **1** we also searched for transition structures that may connect them. A TS shown in Figure 4 was assigned to the reaction **$^3$1a** → **$^3$1c** based solely on the inspection of a single imaginary frequency. IRC calculations in both directions failed to converge. Both UB3LYP and PBE0 techniques predicted a barrier less than 1 kcal mol$^{-1}$ for the downhill reaction **$^3$1a** → **$^3$1c**. When the UMPW1K single-point energies computed on the UB3LYP geometries were used, **$^3$1a** → **$^3$1c** had practically identical energies, but the activation barrier exceeded 7 kcal mol$^{-1}$. The UMPW1K geometry optimization failed to produce a transition structure connecting **$^3$1a** → **$^3$1c**. These results may suggest that interconversion of **$^3$1a** → **$^3$1c** cannot be described as an adiabatic reaction. Analysis of the triplet surface crossing using multiconfigurational methods may be required to gain a better understanding of the triplet excited-state dynamics of **1**.

In addition to **$^3$1a** → **$^3$1c**, the optimize geometry of the third triplet species **$^3$1b** could be obtained at the UB3LYP and UPBE0 levels. **$^3$1a** and **$^3$1b** may be classified as conformers. They differ only in the configuration of the $NO_2$ group, but bear similarity in the naphthalene ring geometry, spin density distribution, and reactivity. The interconversion of **$^3$1a** and **$^3$1b** can be considered in terms of two different mechanisms: rotation around the C−N bond and nitrogen inversion. Using the UB3LYP technique we could locate a transition structure, **TS[$^3$1a−$^3$1b]**, for the latter mechanism, which seems to be more feasible for sterically hindered naphthalenes. However, the UB3LYP method yielded a negative value for the activation energy. When the UMPW1K single-point energies computed at the UB3LYP geometries were used, the reaction **$^3$1b** → **$^3$1a** was found to be thermodynamically favorable by 2.7 kcal mol$^{-1}$ and has an activation barrier of 4.9 kcal mol$^{-1}$. Geometry optimization for **TS[$^3$1a−$^3$1b]** could not reach convergence when the UPBE0 or UMPW1K model in combination with the 6-31+G(d,p) basis set was used.

Vertical excitation energies for the triplet states of **1** were estimated by using TD-DFT calculations at the B3LYP/6-311+G(2d,p) level (see Table 2S, Supporting Information). For the $T_1$ state of **1** and 1NN,[58] we obtained almost identical energies of 55.3 and 54.8 kcal mol$^{-1}$. These values are in excellent agreement with the triplet energy of ∼55 kcal mol$^{-1}$ obtained from experimental data for 1NN.[29,53,55] The vertical excitation energy for the $T_1$ state of 1NN was practically identical to the relative energy based on the B3LYP optimized geometries of the singlet ground state and the first triplet excited state.[58] The TD-DFT excitation energies for the $T_2$ state of **1** and 1NN were also close to each other (67.9 kcal mol$^{-1}$ and 66.5 kcal mol$^{-1}$ for **1** and 1NN), but quite different from the energy of **$^3$1a**. Both the $T_1$ and $T_2$ unrelaxed states of **1** were found to be of mixed nature (see Table 2S and Figure 2S, Supporting Information). However, the $T_2$ state was characterized by dominating contributions from the excitations localized on the nitro group. The data presented in Table 2S (Supporting Information) indicate that a single excitation, HOMO → LUMO, dominates the lowest excited-state both of triplet and singlet multiplicity.

**Triplet Potential Energy Landscape.** Unrestricted calculations with two different hybrid HF-DFT techniques (UB3LYP and UMPW1K) were used to map the potential energy surface of 1-methyl-8-nitronaphthalene in the triplet state. The two methods differ, apart from the functional design, in the amount of the Hartree−Fock exchange that is substantially larger for the MPW1K method. Both hybrid functionals yielded qualitatively

(59) (a) Fournier, Thierry; Tavender, Susan M.; Parker, Anthony W.; Scholes, Gregory D.; Phillips, David. *J. Phys. Chem. A* **1997**, *101*, 5320−5326. (b) Fournier, T.; Scholes, G. D.; Gould, I. R.; Tavender, S. M.; Phillips, D.; Parker, A. W. *Laser Chem.* **1999**, *19*, 397−401.

(60) Takezaki, M.; Hirota, N.; Terazima, M.; Sato, H.; Nakajima, T.; Kato, S. *J. Phys. Chem. A* **1997**, *101*, 5190−5195.

(61) (a) Takezaki, M.; Hirota, N.; Terazima, M. *J. Phys. Chem. A* **1997**, *101*, 3443−3448. (b) Takezaki, M.; Hirota, N.; Terazima, M. *J. Chem. Phys.* **1998**, *108*, 4685−4686.

(62) Manaa, M. R.; Fried, L. E. *J. Phys. Chem. A* **1999**, *103*, 9349−9354.

consistent pictures of the potential energy landscape. However, some quantitative differences worth mentioning were found. The B3LYP method provided higher energies (here and below relative to the energy of **1**) for all the minimum-energy structures except $^3$**1c**. The largest difference between the relative UB3LYP and UMPW1K energies was found for the tricyclic intermediate $^3$**6** (5.5 kcal mol$^{-1}$). A similar inconsistency value of 6.4 kcal mol$^{-1}$ was obtained for **6** in the singlet ground state. As expected, the activation barriers predicted with the use of the UB3LYP functional were generally underestimated in comparison to those calculated with the UMPW1K method. The largest discrepancies (~5 kcal mol$^{-1}$) between activation barriers predicted with the two techniques were obtained for the reactions *E*-$^3$**3b** → $^3$**6** and $^3$**2a** → $^3$**5**. The latter reaction corresponds to the NO release from the triplet diradical $^3$**2a**. It is noteworthy that the B3LYP activation energy for the nitro-nitrite rearrangement in the singlet ground state was underestimated by 6.4 kcal mol$^{-1}$ in comparison to the MPW1K method. Both methods failed to predict the activation barriers for the OH rotation in the *aci*-form isomers $^3$**3**.

This study was focused on the two reaction paths that lead from **1** either to the nitrite or to the nitroso compound. The overall reaction for both pathways was predicted to be thermodynamically favorable in the singlet ground state. Nevertheless the ground-state isomerization of **1** should not occur at ambient conditions because both processes are kinetically prohibited. According to the MPW1K results, the nitro-nitrite rearrangement was characterized by activation energy of 60.7 kcal mol$^{-1}$. Based on our prediction for the *aci*-form to be destabilized by approximately 40 kcal mol$^{-1}$ (see Figure 2), the rate of the [1,7]H-shift should also be negligible in the ground state.

Photoexcitation of **1** is expected to result in a drastic decrease of the activation barriers of the isomerization reactions. For the triplet excited state, unrestricted DFT calculations predicted dramatic changes in the isomerization mechanisms. The nitrite **2** in the triplet state was found to be unstable with respect to dissociation into NO and a methylnaphthoxy radical. The triplet radical pair $^3$**5** comprised of these two radicals has energy comparable to that of **1**. The primary product on a triplet-state reaction pathway corresponding to the nitro-nitrite rearrangement appeared to be a diradical $^3$**2**, which was strongly destabilized relative to the nitro form. Analogous diradicals have been proposed as intermediates in the isomerization of nitroalkenes.[2] We obtained optimized geometries for two stereoisomers, $^3$**2a** and $^3$**2b**, and two transition structures connecting them to $^3$**1a** and $^3$**1b**, respectively. $^3$**2a** was found to be only slightly more favorable than $^3$**2b**, but the activation barrier for its formation was smaller by ~3 kcal mol$^{-1}$. At the B3LYP level, the reaction $^3$**1a** → $^3$**2a** was characterized by endothermicity of 7.9 kcal mol$^{-1}$ and activation energy of 8.6 kcal mol$^{-1}$. Practically the same activation barrier was predicted both at the UBLYP and UMPW1K level when a larger basis set was used for geometry optimization (see Figure 5). On the triplet potential energy surface, the diradical intermediate $^3$**2a** and the radical pair $^3$**5**, which is much more favorable, are separated by a large barrier. We found a triplet TS (**TS**[$^3$**2a**−$^3$**5**]) corresponding to synchronous C−N and N−O bond cleavage in $^3$**2a**. At UMPW1K level, the energy of this TS was by 12.0 kcal mol$^{-1}$ higher than that of $^3$**2a**.

In contrast to the ground state, tautomerization of **1** in the triplet excited state was predicted to be highly exothermic. The [1,7]H-shift product, *Z*-$^3$**3a**, was stabilized by more than 10 kcal mol$^{-1}$ relative to the reactant $^3$**1a**. We located a transition state for the tautomerization of the radical-like triplet $^3$**1a**. The UB3LYP/6-311+G(3df,2p) energy of **TS**[$^3$**1a**−*Z*-$^3$**3a**] optimized at the UB3LYP/6-31G(d) level differed only by 1.2 kcal mol$^{-1}$ from that of $^3$**1a**. To obtain more reliable estimates for the activation energy we optimized the TS geometry using the 6-31+G(d,p) basis set and three different hybrid functionals. The results are presented in Figure 5. The best estimates are expected to be those produced by the UMPW1K technique. At this level of theory, the exothermicity of 16.4 kcal mol$^{-1}$ and activation energy of 4.0 kcal mol$^{-1}$ were predicted for the reaction $^3$**1a** → *Z*-$^3$**3a**.

The data shown in Figures 4 and 5 indicate that tautomerization of **1** in the triplet excited state is very efficient and that other isomerization reactions can hardly compete with the hydrogen shift. Although the absolute values differ substantially, all DFT techniques used predicted a notably smaller barrier for the [1,7]H-shift than for the reactions leading to the diradical intermediates $^3$**2**. When we used the UMPW1K activation barrier and partition functions to calculate the tautomerization rate constant (high-temperature limit of the transition state theory), we obtained a value close to $10^9$ s$^{-1}$. The intramolecular hydrogen shift should therefore take place even if the $^3$**1a** lifetime would be as short as that for the structurally related $T_1$ state of nitrobenzene (~500 ps[61]). It is noteworthy that experimental data for 2NB derivatives provided evidence for the photoinduced isomerization exclusively via the singlet excited state.[18,20] In contrast, both the singlet and triplet excited state have been proposed to participate in the analogous rearrangement of 1-nitro-2-naphthaldehyde to the nitroso acid.[63]

Here, it will be recalled that $^3$**1a** is not the lowest energy triplet of the nitro compound studied. For the more favorable and more polar triplet $^3$**1c**, we could not locate any transition structure connecting it to other isomers of **1**. Moreover, different DFT techniques yielded conflicting data for the interconversion of $^3$**1a** and $^3$**1c**. At this point, we can only speculate about dynamics and mechanism(s) of the population of the triplet excited states of **1**. According to our TD-DFT calculations, the $T_3$ state of a strongly mixed character is intervening between the $S_1$ and $T_2$ states and is only 0.11 eV apart from the singlet state (see Table 2S, Supporting Information). The energy of the unrelaxed $T_2$ state is predicted to be 0.55 eV higher than that of the $T_1$ state. However, structural relaxation may result in substantial lowering the energy and therefore may bring the $T_2$ state very close to $T_1$. It means that the $T_2$ state may be responsible for isomerization of 1-nitronaphthalenes. Our preliminary data for 1-hydroxymethyl-8-nitronaphthalene and several analogues show that the photoreaction quantum yields decreases with solvent polarity.[58] This may be attributed to an increase in the $T_1$−$T_2$ gap due to stabilization of

(63) Dvornikov, A. S.; Taylor, C. M.; Liang, Y. C.; Rentzepis, P. M. *J. Photochem. Photobiol. A* **1998**, *112*, 39−46.

the polar $T_1$ state that is essentially nonreactive. Considering small energy differences, the single-determinant techniques used in this study may be inadequate for analysis of *peri*-substituted nitronaphthalenes. Further studies utilizing multireference techniques are clearly needed to clarify these points.

Taken together our computational data suggest that **1** cannot afford oxycompounds that are typically associated with the nitro-nitrite rearrangement through an adiabatic reaction in the low-lying triplet state. Enhanced photoreactivity of 1NN with a methyl group in the *peri*- or *ortho*-position has therefore to be attributed to the tautomerization reaction. Although there is no reason to believe that the nitro-nitrite rearrangement will be much more efficient in the $T_3$ or higher triplet states, we could not exclude this possibility. There are some experimental data suggesting that higher triplet states are involved in the nitro-nitrite rearrangement of 9-nitroanthracenes.[64] We are currently engaged in experimental and computational studies addressing these issues as well as reactivity of the singlet excited states.

The cyclization of the *aci*-form plays the major role in the mechanism and kinetics of the photoinduced isomerization of 2NB derivatives in aqueous solutions.[12,18−20] Much higher activation barriers for the isomerization of anions in comparison to protonated *aci*-forms are responsible for relatively low rates of the overall reaction at pH ∼5−7 and for specific acid catalysis generally observed for nitrobenzyl compounds.[12,18] The diradical *aci*-form of *peri*-substituted nitronaphthalenes is expected to be much more reactive both as the protonated species and as anion. For the parent compound **1**, we obtained optimized geometries for six stereoisomers of the *aci*-form in the triplet state. The triplet species $^3$**3** are predicted to be conjugated diradicals with the electron spin density largely localized on the two oxygen atoms and endocyclic carbon atoms, $C_5$ and $C_7$. A large activation barrier found for the rotation around the $C_1-C_{11}$ bond in *E*-$^3$**3** confirms strong coupling between the $CH_2$ group and the naphthalene ring. In contrast, rotation around the $C_8-N$ bond encounters only a small barrier. At the UMPW1K level, activation energy of 2.8 kcal mol$^{-1}$ was predicted for the exothermic reaction *E*-$^3$**3b** → *Z*-$^3$**3b**. We also optimized geometries of the two isomers, *Z*-**3b** and *E*-**3b**, in the singlet state. Unfortunately, the singlet wave functions were heavily contaminated by higher spin states. This prevented accurate estimation of the singlet−triplet energy gap. Nevertheless, there is little doubt that these two isomers of the *aci*-form **3** will have the ground state of triplet multiplicity.

According to our DFT calculations, the *aci*-form of **1** is a rather stable intermediate placed well below the first singlet and triplet excited states of the nitro form (see Figure 4 and Table 2S, Supporting Information). On the triplet potential energy surface, large activation barriers separate $^3$**3** from the tricyclic intermediate $^3$**6**, which should lead to the nitroso compound $^3$**4**.[18−21,46] Although our data apply to the gas-phase reactions, we do not expect any dramatic change in the activation barrier for the reaction *E*-$^3$**3** → $^3$**6** in solution. We could not locate a triplet TS for the cyclization affording $^3$**7**, but this reaction seems to be very unlikely considering that the energy of $^3$**7** is by 31.2 kcal mol$^{-1}$ higher than that of *Z*-$^3$**3d**, the least stable isomer of the *aci*-form. Our computational results suggest that triplet *aci*-nitro compounds $^3$**3** react via thermal population of the singlet excited state, which is expected to rapidly cyclize.[58] If the S−T energy gap is not much different from what we obtained after correction for the spin contamination (∼2 kcal mol$^{-}$1), than the T−S intersystem crossing in **3** can hardly affect facile singlet-state isomerization into the nitroso compound. Taken together, the DFT data support the idea that the triplet excited-state plays an important role in the photoinduced decomposition of substituted nitronaphthalenes.

## Conclusions

Rearrangements of 1-methyl-8-nitronaphthalene (**1**) in the triplet state were studied with the DFT-based methods. Similar results for the landscape of the triplet potential energy surface were obtained by using the popular UB3LYP technique and the UMPW1K model specifically optimized for reaction kinetics studies. The UB3LYP activation barriers were generally underestimated in comparison to those provided by the UMPW1K model. Two distinct minima corresponding to the nitro isomer of **1** were located on the triplet surface. These two species were characterized by comparable energies that were close to the vertical excitation energy of the $T_1$ state as predicted by TD-DFT. Two distinct pathways for the isomerization of the triplet nitronaphthalene were analyzed in detail. The activation barriers for the reactions affording nitrite-type diradical intermediates were found to be significantly larger than that for the intramolecular hydrogen shift resulting in the *aci*-form of **1**. The latter reaction was predicted to occur on the nanosecond time scale. The DFT results showed that the diradical *aci*-form of **1** has the ground state of triplet multiplicity. A very large activation energy predicted for the *aci*-form cyclization in the triplet state suggests that this diradical isomerizes mainly via the thermal population of a close-lying singlet excited state, which is expected to be highly reactive. The results obtained pointed out the importance of surface crossing in photoinduced rearrangements of *peri*-substituted nitronaphthalenes. Computational studies currently under way should clarify these issues.

**Acknowledgment** is made to the Donors of the American Chemical Society Petroleum Research Fund for partial support of this research. The support of Kansas NSF Cooperative Agreement EPS-9874732 and the Wichita State University High Performance Computing Center is also acknowledged.

**Supporting Information Available:** Cartesian coordinates for **1**−**7** and transition structures connecting them (ASCII); Table 1S with the total energies, zero-point energies and imaginary frequencies for the transition structures; Table 2S with vertical transition energies; Figure 1S showing the electron spin density; Figure 2S presenting the Kohn−Sham orbitals for **1**. This material is available free of charge via the Internet at http://pubs.acs.org.

JO0509253

(64) (a) Hamanoue, K.; Amano, M.; Kimoto, M.; Kajiwara, Y.; Nakayama, T.; Teranishi, H. *J. Am. Chem. Soc.* **1984**, *106*, 5993−5997. (b) Hamanoue, K.; Hirayama, S.; Nakayama, T.; Teranishi, H. *J. Phys. Chem.* **1980**, *84*, 2074−2078.